

Integrated Water Vapor Field and Multiscale Variations over China from GPS Measurements

SHUANGGEN JIN

Korea Astronomy and Space Science Institute, Daejeon, South Korea

Z. LI

National Geomatics Center of China, Beijing, China

J. CHO

Korea Astronomy and Space Science Institute, Daejeon, South Korea

(Manuscript received 27 November 2007, in final form 27 March 2008)

ABSTRACT

Water vapor plays a key role in the global hydrologic cycle and in climatic change. However, the distribution and variability of water vapor in the troposphere are not understood well—in particular, in China with the complex Tibetan Plateau and the influence of the Asian and Pacific monsoons. In this paper, continuous global positioning system (GPS) observations for 2004–07 in China are used to produce precipitable water vapor (PWV) measurements; these measurements constitute the first investigation of PWV distribution and variability over China. It has been found that the stronger water vapor values are in southeastern China and the lower water vapor values are in northwestern China. These distributions are mainly affected by the latitude, topographical features, the season, and the monsoon. Water vapor variations over China are mainly dominated by seasonal variations. The strong seasonal cycles are in summer with maximum water vapor and in winter with minimum water vapor. The PWV in southeastern China has an annual amplitude of about 15 mm, much larger than in northwestern China at about 4 mm, and meanwhile the time of peak water vapor content is one month earlier than in other regions, probably because of the known rainy season (mei-yu). In addition, significant diurnal variations of water vapor are found over all GPS stations, with a mean amplitude of about 0.7 mm, and the peak value occurs around noon or midnight, depending on geographic location and topographical features. The semidiurnal cycle is weaker, with a mean amplitude of about 0.3 mm, and the first peak PWV value appears around noon.

1. Introduction

Atmospheric water vapor is a variable that interacts with the solar radiation and controls the thermodynamics and energy balance of the atmosphere. Therefore, water vapor plays a key role in the global hydrologic cycle and heat processes of the climate system. Integrated or precipitable water vapor (PWV) is an impor-

tant indicator of water vapor variability in the lower troposphere and related climate processes. It represents the water vapor storage in the column of the atmosphere in terms of water budget, as a result of the balance among precipitation, evaporation, and convergence of humidity (Fontaine et al. 2003). PWV concentrations possess a high degree of spatial and temporal variability that depends on the season, topographic features, and other local and regional climatic conditions, especially in China with the highest Tibetan Plateau and being subject to the Asian and Pacific monsoons. However, the spatial and temporal distribution features of water vapor concentrations were not understood well until radiosonde data became available (Bannon

Corresponding author address: Dr. Shuanggen Jin, Korea Astronomy and Space Science Institute, 61-1, Whaam-dong, Yuseong-gu, Daejeon 305-348, South Korea.
E-mail: sgjin@kasi.re.kr

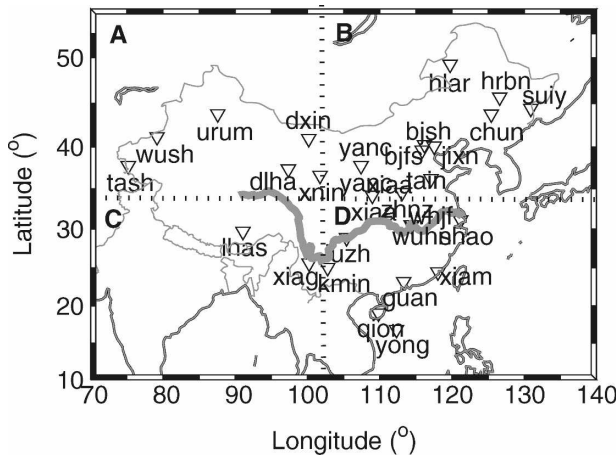


FIG. 1. Distribution of the CMONC GPS sites in China: northwestern China is labeled as A, northeastern China is labeled as B, southwestern China is labeled as C, and southeastern China is labeled as D. The thick line in the middle is the Yangtze River valley.

and Steele 1960; Starr et al. 1965). Although many studies were done with radiosonde data in different regions (e.g., Angell et al. 1984; Hense et al. 1988; Gaffen et al. 1992; Elliott et al. 1995), high-time-resolution observations are limited (e.g., hourly or diurnal variations). Global positioning systems (GPS) have recently been widely developed as all-weather, high-spatial-and-temporal-resolution, low-cost remote sensing systems of the atmosphere (Bevis et al. 1994; Hernández-Pajares et al. 2001), as compared with conventional techniques such as satellite radiometer sounding, ground-based microwave radiometer, and radiosondes (Westwater 1993). With independent data from other instruments—in particular, water vapor radiometers—it has been demonstrated that water vapor can be retrieved using ground-based GPS observations with the same level of accuracy as radiosondes and microwave radiometers (Elgered et al. 1997; Rocken et al. 1993; Duan et al. 1996; Emaradson et al. 1998; Tregoning et al. 1998). Furthermore, GPS-derived water vapor has high resolutions (0.5–2 h). Therefore, GPS can be used to study short-time-scale variations of water vapor as well as its distribution.

The national project “Crustal Movement Observation Network of China” (CMONC) contained a nationwide fiducial network with about 28 continuous GPS observation sites (see Fig. 1). These continuous GPS observations can be used to compute daily station position, PWV, and total electron content, which are used for crustal deformation monitoring, meteorological, and space environments over China. In this paper, the 2-h water vapor field over China is retrieved from continuous GPS observations of the CMONC for 2004–07

and the first use of these data to study PWV distributions and multiscale variations is presented.

2. GPS water vapor retrievals

The available continuous GPS observation data for 2004–07 are processed by Bernese software (Dach et al. 2007) with International GPS Services (IGS) final orbits, International Earth Rotation and Reference Systems Service (IERS) Earth orientation parameters, azimuth- and elevation-dependent antenna phase center models, and newly recommended strategies (Byun et al. 2005; Jin et al. 2007). The unknown parameters contain station coordinates, atmospheric gradient, zenith tropospheric delay (ZTD) every 2 h, GPS satellite orbital parameters, and so on.

The ZTD is the integrated refractivity along a vertical path through the neutral atmosphere:

$$\text{ZTD} = c\tau = 10^{-6} \int_0^{\infty} N(s) ds, \quad (1)$$

where c is the speed of light in a vacuum, τ is the delay measured in units of time, and N is the neutral atmospheric refractivity. The refractivity N is empirically related to standard meteorological variables as (Davis et al. 1985)

$$N = k_1\rho + k_2 \frac{P_w}{Z_w T} + k_3 \frac{P_w}{Z_w T^2}, \quad (2)$$

Where k_i ($i = 1, 2, 3$) are constants given by Bevis et al. (1994), ρ is the total mass density of the atmosphere, P_w is the partial pressure of water vapor, Z_w is a compressibility factor close to unity that accounts for the small departures of moist air from an ideal gas, and T is the temperature in kelvins. The integral of the first term of Eq. (2) is the hydrostatic component N_h , and the integral of the remaining two terms is the wet component N_w . Thus, ZTD is the sum of the hydrostatic or “dry” delay (ZHD) and nonhydrostatic or “wet” delay (ZWD), due to the effects of dry gases and water vapor, respectively. The dry component ZHD is related to the atmospheric pressure at the surface, and the wet component ZWD can be transformed into PWV by the mapping function $\Pi = \{10^{-6} \rho R_v [(k_3/T_m) + k_2']\}^{-1}$, where ρ is the density of liquid water, R_v is the specific gas constant for water vapor, T_m is a weighted mean temperature from $T_m = 70.2 + 0.72T_s$, where T_s is the surface temperature in kelvins (Bevis et al. 1994), $k_2' = k_2 - mk_1$, and m is M_w/M_d , the ratio of the molar masses of water vapor and dry air (Davis et al. 1985). Some GPS sites have a lack of collocated surface temperature and pressure data; the absent surface pressures are interpolated from global 3-h surface synoptic

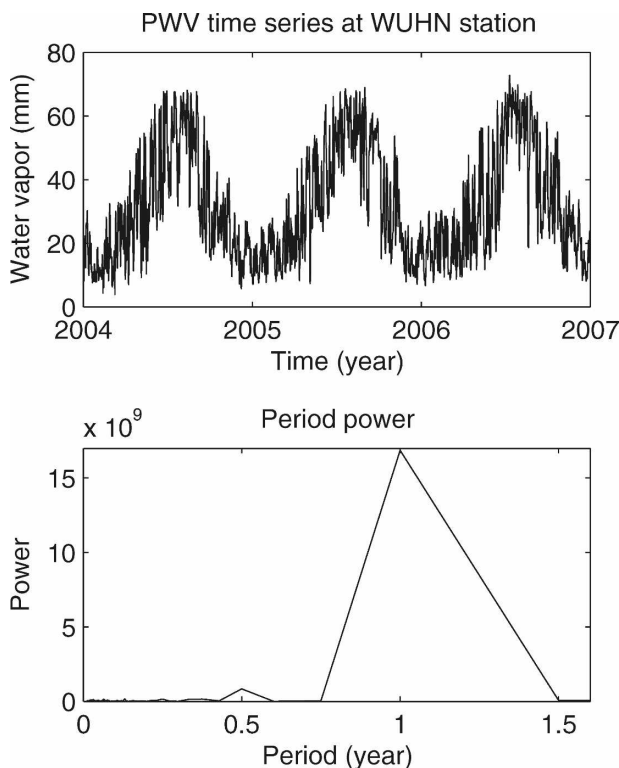


FIG. 2. (top) PWV time series at WUHN station for 2004–07 and (bottom) period power chart.

observations from the Comprehensive Ocean–Atmosphere Dataset (COADS; <http://dss.ucar.edu/datasets/ds464.0>) and the absent surface temperatures are estimated from the 6-hourly National Centers for Environmental Prediction–National Center for Atmospheric Research reanalysis products (<ftp://ftp.cdc.noaa.gov/Datasets/ncep.reanalysis>; Wang et al. 2005). Thus, 2-h PWV time series for 2004–07 over China can be obtained from GPS-derived ZTD and surface pressure and temperature data, and the uncertainty of PWV is about 0.5–1.5 mm because of errors in ZTD, surface pressure, and temperature. For example, Fig. 2 shows the water vapor time series at the Wuhan, China, (WUHN) station for 2004–07. In general, the GPS-derived PWV agrees well with that from radiosonde in Beijing and Shanghai, China, and with collocated very long baseline interferometry (VLBI) observations in Shanghai, with a mean difference of about 1.8 mm and mean root-mean-square (rms) of about 1.5 mm.

3. Results and discussion

a. Water vapor distribution

Precipitable water vapor is a key parameter of the atmosphere and varies with season, topographic features, and other climatic conditions. The 3-yr PWV

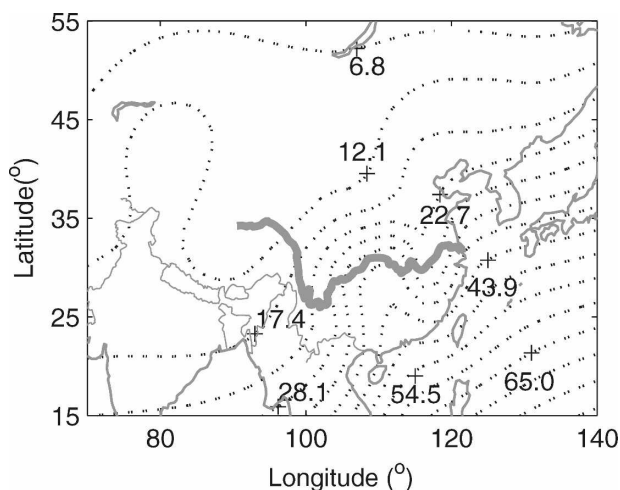


FIG. 3. Contour distribution of mean PWV (mm) over China. The mean PWV at each site was calculated from the 2-h PWV time series over 3 yr. The thick line in the middle is the Yangtze River valley.

time series with 2-h sampling at 28 GPS sites over China provide an important data source to investigate water vapor distribution features and to understand its variability and change. The mean PWV was calculated from the 2-h PWV time series over 3 yr with the sample size of about 12 000 at each station. Figure 3 shows the distribution of mean PWV as a contour with kriging interpolation (Isaaks and Srivastava 1989). Over northern and western China the water vapor content is lower, ranging from 6.8 to 20.0 mm, and over the Yangtze River valley (shown by the thick line in the middle part of Fig. 3) and southeast China it is about 40.0–65.0 mm. It can be seen that the water vapor distribution over China has a latitudinal feature, as typified in the east of

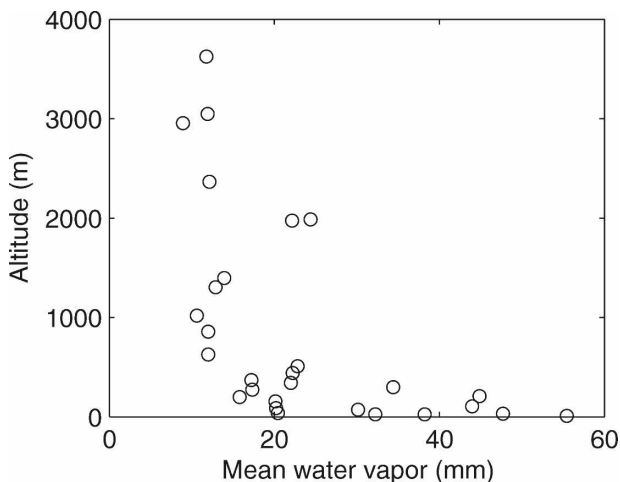


FIG. 4. Distribution of mean PWV with altitude (above global mean sea level). The circles represent the mean PWV at each site.

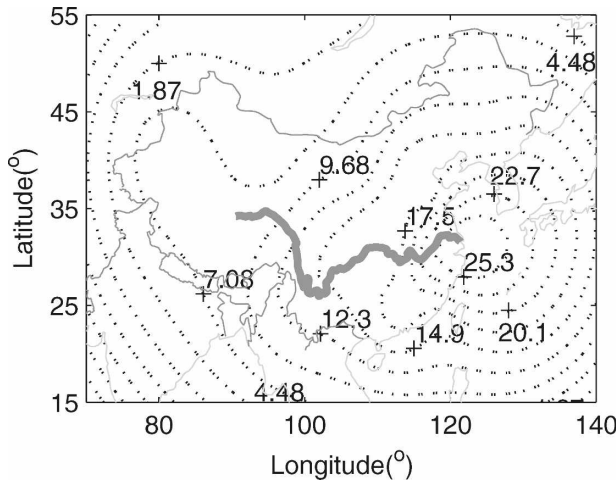


FIG. 5. Contour distributions of annual PWV amplitudes over China.

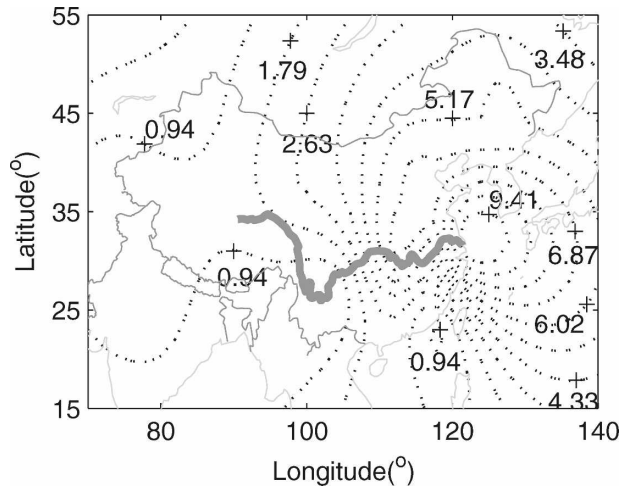


FIG. 7. Contour distributions of semiannual PWV amplitudes over China.

China. As the latitude increases, the water vapor amount decreases, with an obvious difference between southern China and northern China. The distribution features of PWV closely match China's geographical locations and probably reflect the influence of the Asian and Pacific monsoons (Chang 2004). Higher PWV in the southeast of Tibet is due to water vapor transportation from the Bay of Bengal and adjacent areas (Zou et al. 1990). At the same latitude, the water vapor over western China is lower than over eastern China, which may be caused by a colder atmosphere over the high, snow-covered surface over the western areas (e.g., Tibet). Figure 4 shows the distribution of mean PWV with altitude (above global mean sea level). The circle represents the mean PWV at each site, with

uncertainty of 0.5–1.5 mm. An obvious descent of the water vapor content is seen with increasing elevation. Therefore, the distribution of atmospheric water vapor over China is mainly dominated by the latitude, topographical features, and climatic conditions. In addition, because of nonuniform GPS station distribution—in particular, in western China—the interpolated water vapor distribution features need to be further investigated with future denser observations.

b. Seasonal variations of water vapor

We analyzed all of the PWV time series at each GPS station with fast Fourier transform and found that the most marked periods of PWV time series at all GPS

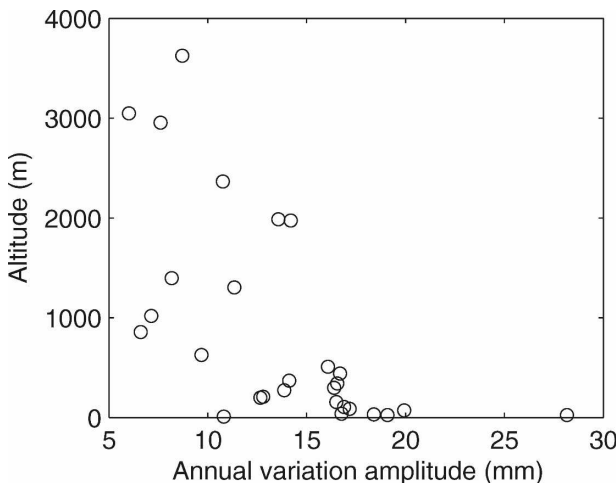


FIG. 6. Distribution of annual PWV variation amplitudes with altitude. The circles represent annual PWV variation amplitude at each site.

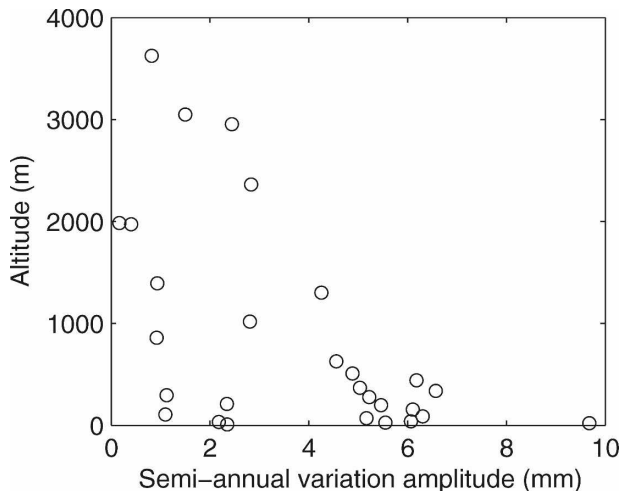


FIG. 8. Distribution of semiannual PWV variation amplitudes with altitude. The circles represent semiannual PWV variation amplitude at each site.

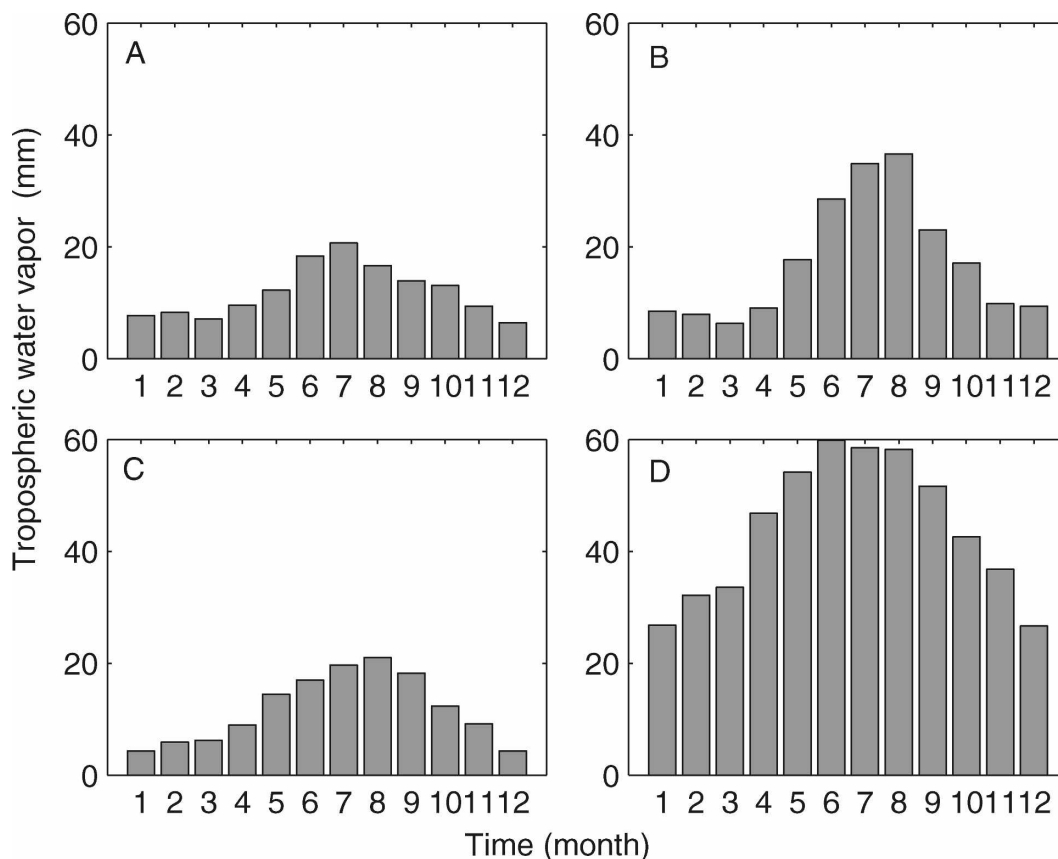


FIG. 9. Distribution of monthly PWV at the four subregions (A–D) marked in Fig. 1.

stations are about 1 and 0.5 yr. For example, Fig. 2 (bottom panel) shows the period power chart of PWV time series at the WUHN GPS site. The strong 1-yr and weak 0.5-yr periods have shown clear significant annual and weak semiannual variations, respectively. The characteristics of annual and semiannual terms at each site are exacted from 3-yr PWV time series. The uncertainty is about 0.7 and 0.4 mm for annual and semiannual amplitudes, respectively. The strong seasonal cycles are in summer with a maximum water vapor because of the influence of a moist summer monsoon and in winter with a minimum water vapor because of cold temperatures and dry weather. Figure 5 shows the amplitude of annual water vapor variations over China. The higher amplitudes are found in mid-eastern China with about 25.3 mm, and the lower amplitudes are focused on western China. The annual-variation amplitudes are closely related to the topographic elevation (see Fig. 6). The semiannual-variation amplitudes are weak, with approximately several millimeters, much lower than annual variations—in particular, in western China with insignificant semiannual variations (Fig. 7) that are also related to the topographic elevation (see Fig. 8).

Based on the topographic features, China is divided into four subregions in Fig. 1 marked as A (northwestern China), B (northeastern China), C (southwestern China), and D (southeastern China). The mean monthly medians of each subregion are obtained from 3-yr PWV time series and are shown in Fig. 9. It can be

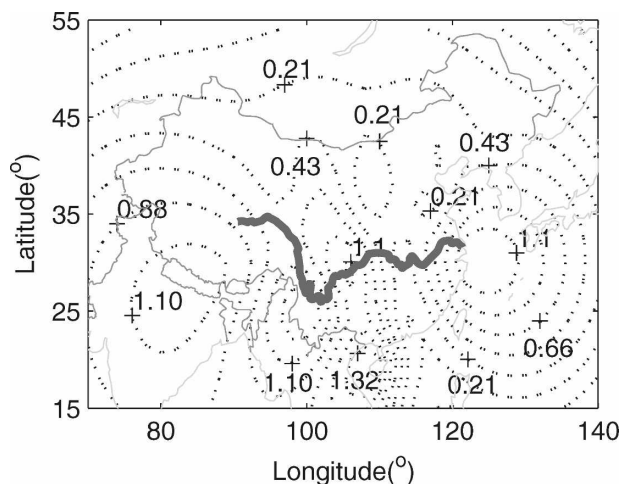


FIG. 10. Contour distributions of diurnal PWV amplitudes over China.

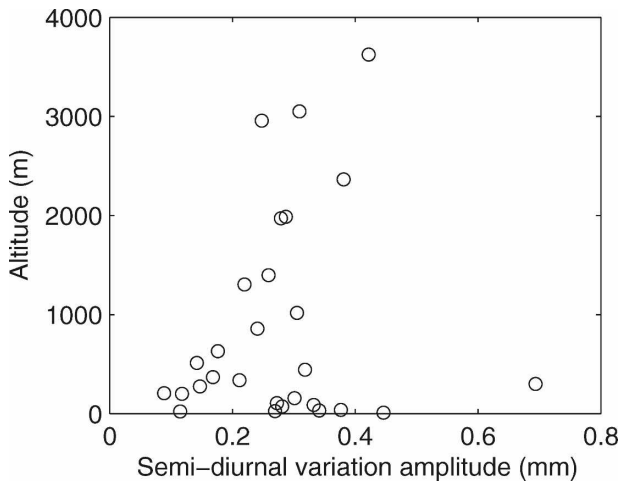


FIG. 11. Distribution of semidiurnal PWV variation amplitudes with altitude. The circles represent semidiurnal PWV variation amplitude at each site.

seen that the higher monthly water vapors are in eastern China (B and D) while western China (A and C) has lower monthly water vapors, but the entire water vapor in each region has a significant seasonal variation. The peak PWV content appears in July–August,

and the minimum PWV value occurs in January in southeastern China. However, the peak PWV values in the western China regions (A and C) are much lower than the minimum value in southeastern China (D). The peak time also has an anomaly in different regions. For example, the time of peak water vapor content in southeastern China (D) is one month earlier than other regions, probably due to the well-known rainy season (mei-yu) in southeastern China. In addition, water vapor in spring is a little lower than in autumn over China, which possibly causes a weak semiannual (i.e., 6-month period) variation of PWV. This difference is also consistent with Peixoto et al. (1981), who found during the study of large-scale atmospheric moisture processes that water vapor levels in spring and autumn are not identical but tend to resemble those in their antecedent seasons.

c. Diurnal variation of water vapor

Significant diurnal (24 h) variations of water vapor are found over all GPS stations, and the mean amplitude is about 0.7 mm with an uncertainty of about 0.1 mm (Fig. 10). The higher elevation has a larger amplitude of diurnal variation, with up to about 1.2 mm. The

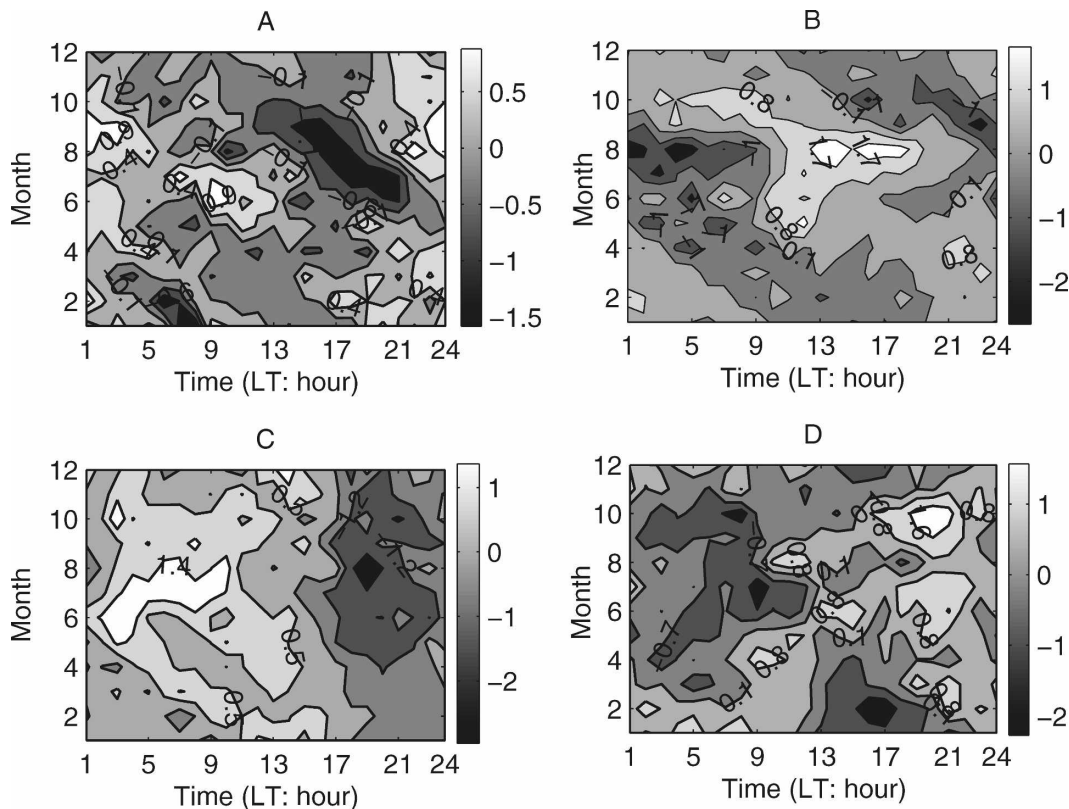


FIG. 12. Mean monthly variations of PWV diurnal cycle anomalies (mm) at the four subregions (A–D) marked in Fig. 1.

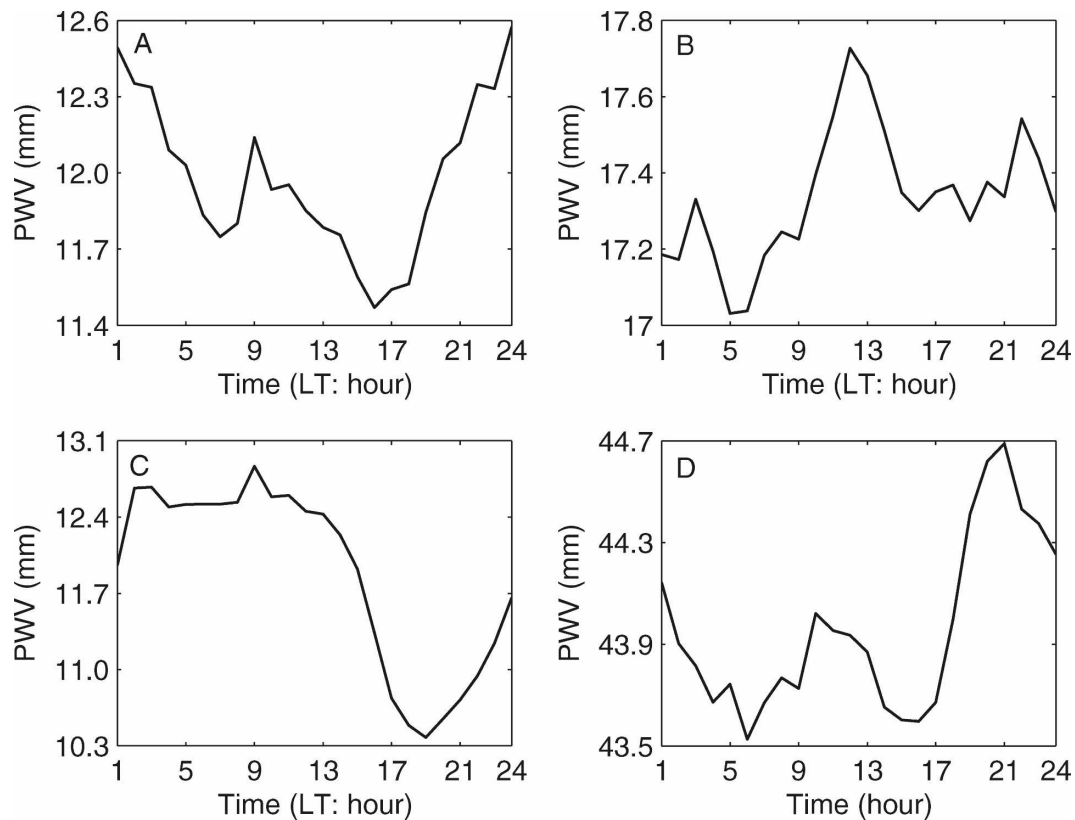


FIG. 13. Mean diurnal variation of PWV at the four subregions (A–D) marked in Fig. 1.

diurnal peak PWV values appear around noon between 0900 and 1300 LT and around midnight between 2000 and 0000 LT, depending on locations, seasons, and so on. The semidiurnal (12 h) cycle is weaker, with an amplitude of normally less than 0.5 mm (excluding one site, Lush, with about 0.7 mm). The larger amplitudes are located at higher elevation areas (Fig. 11). The phase of the semidiurnal cycle is noisier than that of the diurnal variation, and the semidiurnal peak PWV values occur around noon and midnight (for the second cycle). Furthermore, the diurnal and semidiurnal cycles vary with the season. Figure 12 shows the monthly variation of diurnal PWV cycle anomalies at four subregions as marked in Fig. 1. Region C (i.e., Tibet area) has a marked diurnal variation, with the peak time in the morning between 0200 and 1400 LT. The mean diurnal variations of tropospheric water vapor at four subregions are clear to show the diurnal variation features (Fig. 13). The weak semidiurnal oscillations are significant at regions A, B, and D, excluding the winter season (December–February), with a dominant diurnal oscillation. The peak times of semidiurnal oscillations are located in the day between 0900 and 1300 LT and in the night between 2000 and 0000 LT, which may be linked to the diurnal cycle of convection.

4. Conclusions

The 3-yr tropospheric water vapor field is retrieved from continuous GPS observations of the CMONC for 2004–07, which are the first used to investigate the significant variability and distributions over broad and complex geomorphologic China. Distinct seasonal cycles and diurnal variations are found over all GPS stations. The stronger mean water vapors are in southeastern China while northwestern China has lower mean water vapors. The marked seasonal cycles are in summer with a maximum water vapor and in winter with a minimum water vapor. PWV in southeastern China has an annual amplitude of about 15 mm, much larger than in northwestern China with about 4 mm. Meanwhile, the time of peak water vapor content is one month earlier than other regions, probably because of the well-known rainy season (mei-yu). The mean amplitude of significant diurnal variations of water vapor is about 0.7 mm, and the peak diurnal PWV values occur around noon and midnight and are affected by the diurnal cycle of convective activities. The semidiurnal cycle is weaker, with an amplitude of normally less than 0.5 mm and the peak semidiurnal PWV values appear around noon and midnight (for the second

cycle). The spatial distributions and variabilities of PWV are mainly dominated by the latitude, topographical features, the season, and the monsoon. In the future, these PWV datasets will be further applied in numerical prediction models, climatology, and so on.

Acknowledgments. The authors acknowledge the use of GPS data that were retrieved from the Crustal Movement Observation Network of China (CMONC). We also thank the referees for valuable suggestions that significantly improved the article. This work was supported by the Korea Meteorological Administration Research and Development Program under Grant CATER 2006-3104.

REFERENCES

- Angell, J. K., W. P. Elliott, and M. E. Smith, 1984: Tropospheric humidity variations at Brownsville, Texas, and Great Falls, Montana, 1958–80. *J. Climate Appl. Meteor.*, **23**, 1286–1296.
- Bannon, J. K., and L. P. Steel, 1960: Averaged water vapor contents of the air. Geophysical Memo. 102, U.K. Meteorological Office M.O. 631b, 38 pp.
- Bevis, M., S. Businger, S. Chiswell, T. A. Herring, R. A. Anthes, C. Rocken, and R. H. Ware, 1994: GPS meteorology: Mapping zenith wet delays onto precipitable water. *J. Appl. Meteor.*, **33**, 379–386.
- Byun, S. H., Y. Bar-Sever, and G. Gendt, 2005: The new tropospheric product of the International GNSS service. *Proc. ION GNSS Conf.*, Long Beach, CA, Institute of Navigation, 241–249.
- Chang, C. P., 2004: *East Asian Monsoon*. World Scientific, 564 pp.
- Dach, R., U. Hugentobler, P. Fridez, and M. Meindl, 2007: Bernese GPS software version 5.0. Astronomical Institute, University of Bern, 612 pp.
- Davis, J. L., T. A. Herring, I. Shapiro, A. Rogers, and G. Elgered, 1985: Geodesy by radio interferometry: Effects of atmospheric modeling errors on estimates of baseline length. *Radiol. Sci.*, **20**, 1593–1607.
- Duan, J., and Coauthors, 1996: GPS meteorology: Direct estimation of the absolute value of precipitable water. *J. Appl. Meteor.*, **35**, 830–838.
- Elgered, G., J. Johansson, B. Rönnäng, and J. Davis, 1997: Measuring regional atmospheric water vapor using the Swedish Permanent GPS Network. *Geophys. Res. Lett.*, **24**, 2663–2666.
- Elliott, W. P., R. J. Ross, and D. J. Gaffen, 1995: Water vapor trends over North America. Preprints, *Sixth Symp. on Global Change Studies*, Dallas, TX, Amer. Meteor. Soc., 185–186.
- Emardson, T. R., G. Elgered, and J. M. Johansson, 1998: Three months of continuous monitoring of atmospheric water vapor with a network of GPS receivers. *J. Geophys. Res.*, **103**, 1807–1820.
- Fontaine, B., P. Roucou, and S. Trzaska, 2003: Atmospheric water cycle and moisture fluxes in the West African monsoon: Mean annual cycles and relationship using NCEP/NCAR reanalysis. *Geophys. Res. Lett.*, **30**, 1117, doi:10.1029/2002GL015834.
- Gaffen, D. J., W. P. Elliott, and A. Robock, 1992: Relationship between tropospheric water vapor and surface temperatures as observed by radiosondes. *Geophys. Res. Lett.*, **19**, 1839–1879.
- Hense, A., P. Krahe, and H. Flohn, 1988: Recent fluctuations of tropospheric temperature and water vapor in the tropics. *Meteor. Atmos. Phys.*, **38**, 215–227.
- Hernández-Pajares, M., J. M. Juan, J. Sanz, O. L. Colombo, and H. van der Marel, 2001: A new strategy for real-time integrated water vapor determination in WADGPS networks. *Geophys. Res. Lett.*, **28**, 3267–3270.
- Isaaks, E. H., and R. M. Srivastava, 1989: *An Introduction to Applied Geostatistics*. Oxford University Press, 561 pp.
- Jin, S. G., J. U. Park, J. H. Cho, and P. H. Park, 2007: Seasonal variability of GPS-derived zenith tropospheric delay (1994–2006) and climate implications. *J. Geophys. Res.*, **112**, D09110, doi:10.1029/2006JD007772.
- Peixoto, J. P., D. A. Salstein, and R. D. Rosen, 1981: Intra-annual variation in large-scale moisture fields. *J. Geophys. Res.*, **86**, 1255–1264.
- Rocken, C., R. H. Ware, T. Van Hove, F. Solheim, C. Alber, J. Johnson, and M. G. Bevis, 1993: Sensing atmospheric water vapor with the global positioning system. *Geophys. Res. Lett.*, **20**, 2631–2634.
- Starr, V. P., J. P. Peixoto, and A. R. Crisi, 1965: Hemispheric water balance for IGY. *Tellus*, **17**, 463–471.
- Tregoning, P., R. Boers, and D. O'Brien, 1998: Accuracy of absolute precipitable water vapor estimates from GPS observations. *J. Geophys. Res.*, **103**, 701–710.
- Wang, J., L. Zhang, and A. Dai, 2005: Global estimates of water-vapor-weighted mean temperature of the atmosphere for GPS applications. *J. Geophys. Res.*, **110**, D21101, doi:10.1029/2005JD006215.
- Westwater, E. R., 1993: Ground-based microwave remote sensing of meteorological variables. *Atmospheric Remote Sensing by Microwave Radiometry*, M. A. Janssen, Ed., John Wiley and Sons, 145–213.
- Zou, J. S., J. Jiang, and M. H. Huang, 1990: *Upper-Air Climatology*. Meteorological Press, 239 pp.